

Stored Energy in Nickel Cold Rolled to Large Strains, Measured by Calorimetry and Evaluated from the Microstructure

T. KNUDSEN, W.Q. CAO, A. GODFREY, Q. LIU, and N. HANSEN

High-purity polycrystalline nickel (99.99 pct purity) was cold rolled to equivalent von Mises strains from 1.4 to 4.5 (70 to 98 pct reduction in thickness). The stored energy of the deformed samples was measured using both microstructural parameters obtained from transmission electron microscope (TEM) investigations and differential scanning calorimetry (DSC). For the microstructure-based estimate of the stored energy, the required parameters are the misorientation angles across, and the spacings between the dislocation boundaries and high-angle boundaries present after deformation. It was found that the stored energy determined from both TEM and DSC investigations increased linearly with strain, with the latter being larger by a factor of between 1.9 and 2.7. This difference can be reduced by considering the contribution to the stored energy from other sources.

DOI: 10.1007/s11661-007-9421-1

© The Minerals, Metals & Materials Society and ASM International 2008

I. INTRODUCTION

THE processing of metals by plastic deformation requires mechanical energy, of which only a small fraction is stored in the metal in the form of dislocations, point defects, high-angle boundaries, and, in some materials, twins.^[1] The stored energy can be measured directly by calorimetry^[1,2,3–11] or it can be estimated based on a microstructural characterization.^[12–14] In recent studies, the correlation between the stored energy of the deformation and the characteristics of the deformed microstructure has been analyzed.^[12,14] In these studies, it has been shown that the stored energy can be estimated by applying the Read–Shockley equation to the boundaries observed in the deformed microstructure. Note that, in this article, we use the term “dislocation boundaries” to refer to boundaries with a misorientation angle of less than 15 deg, and the term “high-angle boundaries” to denote all other boundaries in the microstructure (including the original grain boundaries and those boundaries with a misorientation angle > 15 deg formed during deformation). For aluminum, it has been observed that there is a relationship between the stored energy and both the applied strain and the flow stress after deformation.^[12] The topic of stored energy is of general importance in various

materials science fields, including, for example, recovery, recrystallization, and crystal plasticity. The correct estimation of the stored energy in a deformed metal is, therefore, crucial when analyzing and modeling such phenomena.

The objective of the present study is to supplement the microstructure-based method by measuring the stored energy directly by differential scanning calorimetry (DSC). This permits analysis of the question of whether other sources of stored energy exist in addition to the energy stored in the form of dislocations and high-angle boundaries. Studies with a similar objective have been carried out previously by combining calorimetry, dislocation density measurements by using transmission electron microscopy, and X-ray line broadening.^[15,16] These earlier studies were focused on single crystals of copper deformed in tension to low and medium strains. In contrast, the present study concentrates on polycrystalline nickel samples deformed by cold rolling to a thickness reduction of 70 to 98 pct ($\epsilon_{vM} = 1.4$ to 4.5). At these large strains, linear work hardening (stage IV) dominates. The calorimetric measurements have been carried out by the annealing of high-purity (99.99 pct) nickel, which is chosen in preference to the aluminum used in the previous studies,^[12,13] in order to optimize the precision of the calorimetric measurements. The reason for this is that the heat release in pure nickel is predominantly caused by recrystallization over a fairly narrow temperature range, whereas in aluminum, the heat release is caused by both recovery and recrystallization and takes place over a large temperature interval.^[1] Furthermore, the stored energy in nickel is approximately 5 to 10 times larger than the stored energy in aluminum for an equivalent strain.^[1]

As part of the present investigation, the stored energy of high-purity copper (99.99 pct purity) was also determined. The copper was used as an internal standard,^[3] allowing the precision of the DSC measurements to be estimated by comparison with previous measurements

T. KNUDSEN, Ph.D. Student and N. HANSEN, Doctor Techn., are with the Center for Fundamental Research: Metal Structures in Four Dimensions, Risø National Laboratory, Roskilde, Denmark. Contact e-mail: tine.knudsen@risoe.dk W.Q. CAO, formerly Ph.D. Student with the Department of Materials Science and Engineering, Tsinghua University, Beijing, P.R. China, is currently Post Doctor, with the Department of Materials Engineering, Monash University, Monash, VIC 3800, Australia. A. GODFREY Professor, is with the Department of Materials Science and Engineering, Tsinghua University, Beijing, China. Q. LIU, Professor, is with the Department of Materials Science and Engineering, Chongqing University, Chongqing, P.R. China.

Manuscript submitted May 15, 2007.

Article published online January 3, 2008

conducted in house as well as at other laboratories. For copper of this purity, it has previously been shown by DSC^[4] that the energy release is related to recrystallization, *i.e.*, the heat flow curve shows only one stage. This behavior makes Cu a very suitable material to be used as a standard.

II. EXPERIMENTAL

High-purity polycrystalline nickel (99.99 pct purity) with a grain size of 80 to 100 μm was cold rolled to thickness reductions of 70 pct ($\epsilon_{vM} = 1.4$), 90 pct ($\epsilon_{vM} = 2.7$), 95 pct ($\epsilon_{vM} = 3.5$), and 98 pct ($\epsilon_{vM} = 4.5$), as described in Reference 17. The microstructural parameters were obtained from a previous study in which thin foils were examined in a JEOL* 2000FX

*JEOL is a trademark of Japan Electron Optics Ltd., Tokyo.

transmission electron microscope (TEM) operated at 200 keV. The misorientations were calculated from the analysis of convergent-beam Kikuchi patterns.^[17] The deformed nickel was stored a long time at RT, before the DSC analysis at Risø. To examine whether this storage had any effect, some newly deformed nickel samples were also analyzed in a parallel experiment at Tsinghua University. As will be shown later, no significant difference was found between the two data sets.

High-purity polycrystalline copper (99.99 pct purity) with an average grain size of 25 μm was cold rolled 90 pct ($\epsilon_{vM} = 2.7$), as described in Reference 3, and was used to validate the stored-energy measurements. The copper material and samples were stored in a freezer at -30°C prior to the DSC analysis.

For the DSC measurements, samples of nickel cold rolled 95 and 98 pct and copper cold rolled 90 pct were prepared from the rolled sheets, by punching out disks with a diameter of 6 mm. The deformation introduced by the punching was removed by polishing the disks on silicon-carbide paper (grit 1000/4000), to give a maximum diameter of 4.5 mm (the maximum allowable diameter of the sample pan in the DSC equipment). Samples of material cold rolled 90 and 70 pct were prepared from the rolled sheets by cutting square-shaped samples (approximately 5×5 mm) on an ACCUTOM-5 (Struers Ballerup, Denmark), using the lowest cutting rate and water cooling. Disk-shaped samples with a diameter of 4.5 mm were then obtained by polishing on silicon-carbide paper (grit 1000/4000).

The samples were prepared in order to maximize the amount of material per sample, given the constraint on the sample diameter; hence, the sample weight varied from 35 to 400 mg. The surface of each sample was polished, in order to enhance the heat conductivity between the sample and the sample pan, and was cleaned after polishing in an ultrasonic bath of ethanol. Before use, the aluminum sample pans were heat treated at 500°C for 1 hour.

The DSC measurements (Risø) were carried out in a heat flux calorimeter from Seiko Instruments Inc., Japan

(DSC 120), with the data analysis conducted using the accompanying software. Note that the exothermic peaks are displayed positive. The experiments were conducted with a constant heating rate of 5 K/min, in an inert atmosphere of argon (100 mL/min), with a fully annealed sample as the reference.

The nickel samples were heated from room temperature (RT) to well above the recrystallization temperature: 500°C for the lowest-strain and 475°C for the highest-strain samples. The copper samples were heated from RT to 350°C . Two consecutive measurements were conducted on each sample. This was done in order to ensure that the sample was fully recrystallized and to obtain a baseline for the quantitative measurements. Three samples were examined at each strain level for the nickel; two samples were examined for the copper material.

Additional nickel samples were prepared at Tsinghua University by cold rolling high-purity nickel (99.99 pct purity) to reductions of 70 pct ($\epsilon_{vM} = 1.4$), 90 pct ($\epsilon_{vM} = 2.7$), 93 pct ($\epsilon_{vM} = 3.1$), 96 pct ($\epsilon_{vM} = 3.7$), and 98 pct ($\epsilon_{vM} = 4.5$). One sample per strain was prepared by spark cutting 3-mm square-shaped samples (10 to 30 mg) from the rolled sheets. The stored energy was measured using power-compensated DSC (Perkin-Elmer Inc., Wellesley, USA). The specimens were heated at 10 K/min from RT to 500°C , in an inert atmosphere.

Nickel samples for yield stress measurement were also prepared at Tsinghua University. For these samples, 99.99 pct pure nickel was cold rolled to thickness reductions of 10 pct ($\epsilon_{vM} = 0.12$), 20 pct ($\epsilon_{vM} = 0.26$), 37 pct ($\epsilon_{vM} = 0.53$), 50 pct ($\epsilon_{vM} = 0.8$), 70 pct ($\epsilon_{vM} = 1.4$), 90 pct ($\epsilon_{vM} = 2.7$), and 98 pct ($\epsilon_{vM} = 4.5$). From the rolled sheets, tensile specimens were machined, with the tensile direction parallel to the rolling direction. The tensile experiments were conducted in an Instron stress rig (Instron, Norwood, USA). The yield stress values were determined at 0.2 pct plastic deformation.

For comparative purposes, the stored energy of copper cold rolled 90 pct and nickel cold rolled 95 pct (both samples from Risø), have also been measured by the NETZSCH Application Laboratory (Selb, Germany). These samples are denoted as NETZSCH samples here. The stored-energy measurements were conducted in a heat flux DSC (NETZSCH model STA 449 C Jupiter, Netzsch Selb, Germany), at heating rates of either 5 or 50 K/min. The temperature programs, sample pans, gas, and gas flow were as used at Risø.

III. RESULTS

A. Stored Energy—DSC

Figure 1 shows two weight-normalized heat flow curves obtained for a copper sample cold rolled 90 pct. The upper curve is obtained during the first heating ramp, while the lower curve is obtained during reheating of the recrystallized sample. By comparing the two curves, two features appear: (1) a single exothermic peak is observed, which is initiated at 180°C , and (2) a slight difference is observed between the two curves in the temperature interval 50°C to 350°C .

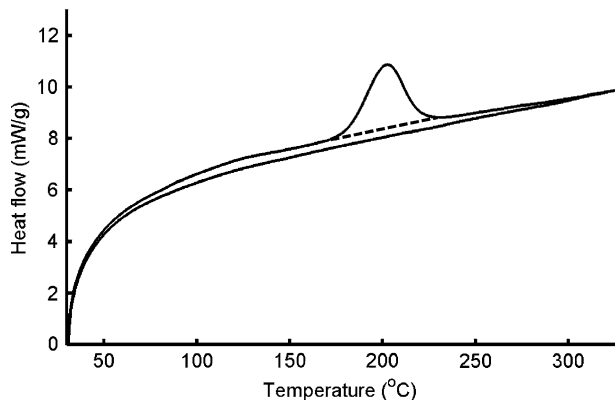


Fig. 1—Heat flow vs temperature of copper cold rolled 90 pct.

The single exothermic peak is related to recrystallization of the sample; the heat released during the recrystallization is obtained by integration of this peak: (1) for the curve in Figure 1, the integration of the peak, *i.e.*, the area enclosed by the curve and the dashed line, gives a stored energy of 0.76 J/g; and (2) a slight difference is observed between the two curves in the temperature interval 50 °C to 350 °C.

Regarding the differences in the energy release curves, if recrystallization is the only process leading to heat release, the two curves should overlap everywhere except for the recrystallization peak region. If heat is released by recovery during the heating ramp, then a higher heat flux during the first heating ramp compared to the second will be seen. However, if recovery were the only reason for the difference in the temperature interval 50 °C to 350 °C, the difference between the two curves would increase with increasing temperature and would be negligible after recrystallization. Since the difference in the signal is nearly constant in this temperature interval, the difference cannot be attributed only to recovery. The observed difference, therefore, might also be of an experimental character—for example, if the heat conduction conditions change after annealing and cooling of the sample. Regardless of the origin of the small differences between the two curves, the main energy release is observed during recrystallization, and this is used to characterize the stored energy of copper.

Figure 2 shows two heat flow curves for a nickel sample cold rolled 95 pct. During the first heating ramp, two exothermic peaks, one large and one small, are observed. The large peak is observed in the temperature interval 280 °C to 385 °C, while the small peak is observed superimposed on the large peak at 358 °C. The large peak is due to the recrystallization of nickel, while the small peak is associated with the energy release during the magnetic transition of nickel. This transition is observed due to a slight difference in the heat capacity (weight) of the sample and the reference (nominally 5 mg, for the data shown in Figure 2).

In the evaluation of the energy stored in nickel due to deformation, the contribution from the magnetic transition has to be subtracted. This energy is found by integrating the small peaks on both the first and second heating curve (illustrated in the insert of Figure 2(b)).

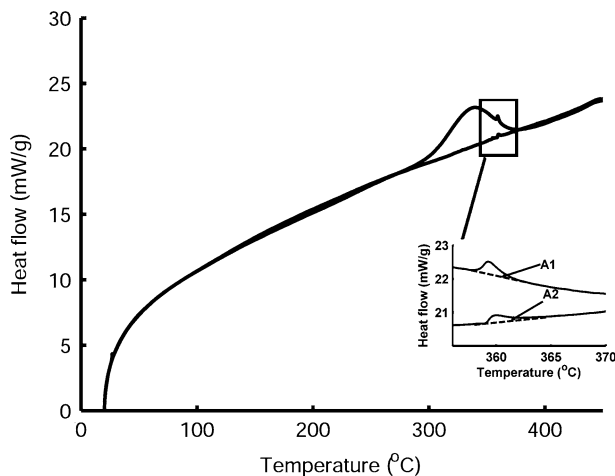


Fig. 2—Heat flow vs temperature of nickel cold rolled 95 pct.

The average value of the two measurements is then taken as the energy associated with the magnetic transition. The energy stored due to deformation is found by integrating the heat flow curve from 280 °C to 385 °C and then subtracting the energy contribution from the magnetic transition. In Figure 2, the energy release from 280 °C to 385 °C is 1.54 J/g, while the energy of the magnetic transition is 0.008 J/g; hence, the energy stored due to deformation in this nickel sample cold rolled 95 pct is 1.53 J/g. All curves were corrected in a similar manner. The two heat flow curves in Figure 2 show nearly no signal difference between the first and second heating ramps in the temperature range outside the recrystallization peak. The main part of stored energy is released, therefore, during recrystallization, and the peak related to recrystallization can be used to determine the stored energy of the nickel samples.

The calorimetric measurements were validated using the copper samples. Two samples have been measured at Risø and one sample at NETZSCH.** The data are

**In the NETZSCH evaluation, the recrystallization peak was also used to characterize the stored energy in copper.

presented in Table I, in which the mean, the standard deviation (σ), and the standard error of the mean ($SE = \sigma \times N^{-0.5}$) are given. The Risø measurements give an average stored energy of 0.77 J/g, equivalent to 6.88 MJ/m³ ($SE = 0.13$ MJ/m³). The NETZSCH measurements give a stored energy of 6.70 MJ/m³, *i.e.*, just 2.6 pct lower than the Risø measurements. This is considered as a very good agreement.

Stored-energy data obtained from all the nickel samples are also shown in Table II. The standard deviation of the Risø experiments is, in this case, 10 to 13 pct. This is significantly higher than for the copper samples; the origin of this is yet to be explored. The standard error of the Tsinghua data is estimated to be 10 pct, based on the upper limit of the standard error of the Risø data.

Table I. Stored Energy of 90 Percent Cold-Rolled Copper

	Risø	NETZSCH
E_{DSC} (J/g)	0.77	0.75
σ	0.015	—
E_{DSC} (MJ/m ³)*	6.88	6.70
σ	0.13	—
SE	0.09	—

*Density of copper: 8933 kg/m³.^[18]

From Table II, it is possible to compare the Risø data with the NETZSCH data. In nickel cold rolled 95 pct, the stored energy measured at Risø is 14.2 MJ/m³, while the NETZSCH determined value is 14.7 MJ/m³. This corresponds to the NETZSCH measurement being 3.5 pct higher than the Risø measurement; hence, these data are also in very good agreement.

The effect of heating rate is demonstrated in Table III, where data obtained at heating rates of 5 and 50 K/min are listed (only one sample has, however, been examined at each rate). If energy is released due to recovery prior to recrystallization, it can be expected that an increase in the heating rate will give an increase in the stored energy measured from the recrystallization peak. Given the small difference in the obtained values (Table III), it is concluded that the present experiment shows no influence from the heating rate. Consequently, the data obtained at Risø with a heating rate of 5 K/min are directly comparable to the data obtained at Tsinghua, where a heating rate of 10 K/min was used.

The nickel stored-energy data are displayed in Figure 3, together with error bars showing the standard error. From the figure, it is seen that the Risø data display a linear increase of stored energy with strain, though some deviation is seen for the measurement conducted at the highest strain. This deviation may be related to experimental error, as samples at these reductions are very thin and light (32 to 37 mg). A small sample mass could, for example, lead to a lower pressure between the sample and the sensor and, consequently, to a large experimental error.

The stored-energy data from the measurements conducted at Tsinghua are also displayed in Figure 3.

Table III. Stored Energy Measured at Different Heating Rates

Sample	ϵ_{vM}	Heat Rate (K/min)	E_{DSC} (MJ/m ³)	Difference
Cu	2.7	5	6.73	—
Cu	2.7	50	6.77	0.6 pct
Ni	3.5	5	14.7	—
Ni	3.5	50	14.95	1.7 pct

A similar linear dependence between stored energy and strain is found, except for a higher stored energy for the highest strain sample. Furthermore, it is noted that the Risø and Tsinghua data agree reasonably well, given the estimated experimental errors. In Figure 4, the weighted averages of all data are plotted as a function of strain, excluding, however, the 93 and 96 pct measurements, as only one measurement was conducted at each of these strains. Figure 4 shows that the weighted average of the measured stored energies (E_{DSC}) increases linearly with strain (ϵ_{vM}) in the entire strain interval, following a relationship given by E_{DSC} (MJ/m³) = 2.3 ϵ_{vM} + 5.9. The weighted average of the measured stored energies is used in the subsequent analysis: the data are given as E_{DSC} in Table V.

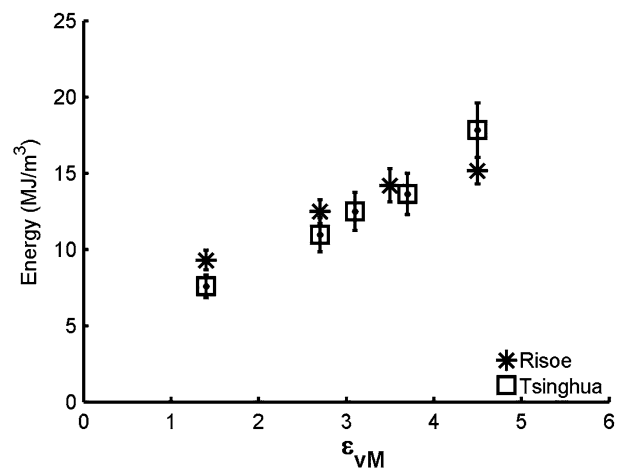


Fig. 3—Stored energy measured with DSC as a function of strain.

Table II. Stored Energy of Cold-Rolled Nickel

Laboratory	Thickness Reduction (Pct)	ϵ_{vM}	E_{DSC} (J/g)	σ (J/g)	SE (J/g)	E_{DSC} (MJ/m ³)*	σ (MJ/m ³)*	SE (MJ/m ³)*
Risø	70	1.4	1.04	0.12	0.07	9.3	1.1	0.64
Risø	90	2.7	1.4	0.15	0.09	12.5	1.3	0.78
Risø	95	3.5	1.59	0.21	0.12	14.2	1.89	1.09
Risø	98	4.5	1.70	0.17	0.09	15.1	1.5	0.86
NETZSCH	95	3.5	1.65	—	—	14.7	—	—
Tsinghua	70	1.4	0.85	—	0.13	7.6	—	1.1
Tsinghua	90	2.7	1.23	—	0.18	11.0	—	1.7
Tsinghua	93	3.1	1.4	—	0.21	12.5	—	1.9
Tsinghua	96	3.7	1.53	—	0.23	13.6	—	2.0
Tsinghua	98	4.5	2.0	—	0.30	17.8	—	2.7

*Density of nickel 8907 kg/m³.^[18]

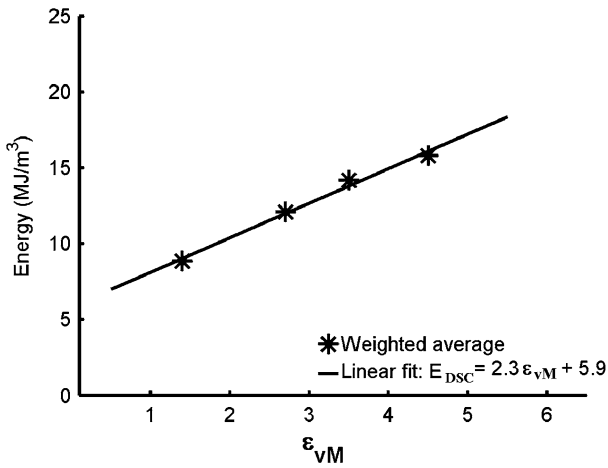


Fig. 4—Weighted average of the stored energy measured with DSC as a function of strain.

B. Stored Energy—TEM

The microstructural parameters used for estimation of the stored energy were obtained from an earlier TEM investigation of cold-rolled high-purity nickel (99.99 pct).^[17,19] The deformed microstructure is subdivided by extended boundaries (geometrically necessary boundaries (GNBs)) and by short interconnecting boundaries (incidental dislocation boundaries (IDBs)), which together form a cell block structure. Between the GNBs and IDBs, a loose dislocation structure is present with a fairly low dislocation density. The average spacing between the boundaries (d_{av}^{IDB} , d_{av}^{GNB}), the distribution of misorientation angles, and the average misorientation angles (θ_{av}^{IDB} , θ_{av}^{GNB}) across the boundaries were determined from longitudinal sections of the cold-rolled samples (Figure 5). The average parameters from these TEM measurements are summarized in Table IV. A number of high-angle boundaries (defined as boundaries with a misorientation angle > 15 deg) are present in the microstructure. For example, after a 70 pct reduction, 7 pct of the 325 analyzed boundaries are high-angle boundaries, while in the sample cold

Table IV. Microstructural Parameters and Estimated Stored Energy for Cold-Rolled Nickel^[20]

Reduction	70 Pct	90 Pct	98 Pct
Strain	1.4	2.7	4.5
θ_{av}^{IDB}	2.2	2.7	3.0
θ_{av}^{GNB}	7.9	14.8	19.7
d_{av}^{IDB} (μm)	0.42	0.39	0.31
d_{av}^{GNB} (μm)	0.28	0.21	0.13
S_V^{IDB} (μm^{-1})	3.10	3.13	3.95
S_V^{GNB} (μm^{-1})	4.36	5.82	9.19
χ (θ_{av}^{IDB})	1.05	1.05	1.05
χ (θ_{av}^{GNB})	1.08	1.08	1.05
$E_{IDB,av}$ (MJ/m ³)	1.09	1.26	1.70
$E_{GNB,av}$ (MJ/m ³)	3.02	4.66	7.58
$E_{TEM,av}$ (MJ/m ³)	4.12	5.93	9.28
$E_{TEM,dist}$ (MJ/m ³)	3.29	4.88	8.16

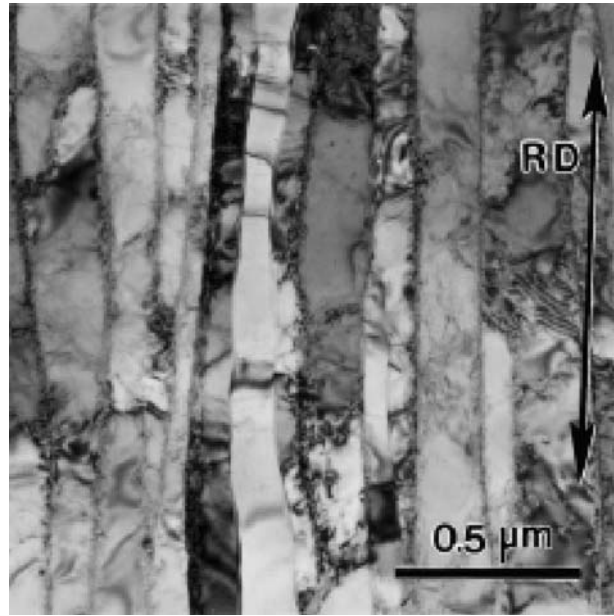


Fig. 5—Microstructure of nickel cold rolled 98 pct, longitudinal section, from Ref. 17.

rolled 98 pct, this figure increases to 28 pct of 410 analyzed boundaries.

If we assume that the total energy stored (E) in a deformation microstructure is due only to the dislocations left behind after deformation, then the stored energy is given by the energy of a dislocation line per unit length (E_{dis}) times the density of dislocations (ρ); *i.e.*,

$$E = \rho \cdot E_{dis} \quad [1]$$

The presence of dislocations in boundaries with misorientations from very small to large angles makes it impossible, however, to determine the dislocation density directly. Hence, an estimate of the stored energy in the deformation structures cannot be made simply by using the relationship given in Eq. [1]. If it is assumed, however, that the dislocations are arranged in low-energy dislocation structures (LEDS), the energy of a given boundary per unit area (γ) is related to the misorientation angle (θ) of the boundary through the Read-Shockley equation:^[12,20]

$$\gamma = \gamma_m \left(\frac{\theta}{\theta_m} \right) \left[1 - \ln \left(\frac{\theta}{\theta_m} \right) \right] : \theta < \theta_m$$

$$\gamma = \gamma_m : \theta \geq \theta_m \quad [2]$$

where γ_m is taken as the grain-boundary energy per unit area for nickel 0.87 Jm^{-2} ,^[21] and θ_m is taken as 15 deg .^[12]

The stored energy of a deformation microstructure (E_{TEM}) can, therefore, be evaluated as the boundary energy per unit area multiplied by the area per volume fraction (S_V) of the boundaries, *i.e.*,

$$E_{TEM} = S_V \cdot \gamma \quad [3]$$

As described previously, the nickel-deformed microstructure contains two boundary types: GNBs and

IDBs. The three-dimensional (3-D) arrangement of the GNBs and IDBs differ. The IDBs consist of cell boundaries with a nearly equiaxed configuration. The IDBs are enclosed by the GNBs, which are extended parallel planar dislocation boundaries. This stereological difference has to be taken into consideration when the area per volume fraction is evaluated from the average spacing (d) of the two boundaries. In References 22 and 23, it is shown that the area per volume fraction of infinitely long GNBs (S_V^{GNB}) and of IDBs (S_V^{IDB}) can be evaluated from the average spacings (d^{GNB} , d^{IDB}) according to

$$S_V^{\text{GNB}} = \frac{1}{d^{\text{GNB}}}; S_V^{\text{IDB}} = \frac{\pi}{2 \cdot d^{\text{IDB}}} \quad [4]$$

This is, however, an idealized description of the microstructure. In reality, the GNBs are not infinitely long, but terminate to form cell blocks. In the evaluation of S_V , an extra contribution from the cell-block ends has to be added to S_V^{GNB} , and this contribution has to be subtracted from S_V^{IDB} . Values of S_V^{IDB} and S_V^{GNB} taking this into account are reported in Reference 19, and the values given there are used in the current calculations (Table IV).

From the microstructural parameters determined in the TEM, it is, therefore, possible to calculate the energy stored in the structure by the use of Eq. [3], in which the two boundary types are considered separately; *i.e.*,

$$E_{\text{TEM}} = S_V^{\text{GNB}} \cdot \gamma^{\text{GNB}} + S_V^{\text{IDB}} \cdot \gamma^{\text{IDB}} \quad [5]$$

where γ^{GNB} is the energy per unit area of the GNBs and γ^{IDB} is the energy per unit area of the IDBs, calculated from Eq. [2]. The stored-energy calculations were conducted in two slightly different ways. In the first method, the average spacings and average misorientations ($\theta_{\text{av}}^{\text{GNB}}$, $\theta_{\text{av}}^{\text{IDB}}$) from Reference 19 are used. Use of the average of the misorientation angles leads, however, to an overestimate of the total stored energy.^[12] To account for this overestimate, the average misorientation angle is, therefore, corrected by a scaling factor χ , defined in Eq. [10] in Reference 12. The scaling factor for GNBs, $\chi(\theta_{\text{av}}^{\text{GNB}})$, and IDBs, $\chi(\theta_{\text{av}}^{\text{IDB}})$, are given in Table IV. The stored energy calculated using the first method ($E_{\text{TEM,avg}}$) is therefore given by

$$E_{\text{TEM,avg}} = S_V^{\text{GNB}} \frac{\gamma(\theta_{\text{av}}^{\text{GNB}})}{\chi(\theta_{\text{av}}^{\text{GNB}})} + S_V^{\text{IDB}} \frac{\gamma(\theta_{\text{av}}^{\text{IDB}})}{\chi(\theta_{\text{av}}^{\text{IDB}})} \quad [6]$$

where $\gamma(\theta_{\text{av}}^{\text{GNB}})$ is the boundary energy per unit area for GNBs, calculated from the average misorientation angle of the boundaries and, likewise, $\gamma(\theta_{\text{av}}^{\text{IDB}})$ is the boundary energy per unit area for IDBs. In the second method, the distributions of the misorientation angles are considered in the calculation of the boundary energy per unit area, as explained here. The misorientation angle data are given in Reference 19 as histograms. From each bin in the histograms are both the average misorientation angles calculated ($\bar{\theta}_{\text{bin}}^{\text{GNB}}$, $\bar{\theta}_{\text{bin}}^{\text{IDB}}$) by and the corresponding boundary energy per unit area found ($\gamma_{\text{bin}}^{\text{GNB}}(\bar{\theta}_{\text{bin}}^{\text{GNB}})$, $\gamma_{\text{bin}}^{\text{IDB}}(\bar{\theta}_{\text{bin}}^{\text{IDB}})$) by the use of Eq. [2]. The

stored energy in one bin is calculated by multiplying $\gamma_{\text{bin}}^{\text{GNB}}(\bar{\theta}_{\text{bin}}^{\text{GNB}})$ (or $\gamma_{\text{bin}}^{\text{IDB}}(\bar{\theta}_{\text{bin}}^{\text{IDB}})$) with the boundary area per volume of the bin ($S_{V-\text{bin}}$), as given by Eq. [3], and the total stored energy associated with one boundary type is found by summing the contribution from all bins in the histogram. Finally, the total stored energy ($E_{\text{TEM,dist}}$) at each strain is given by the sum of contributions from each of the boundary types (GNBs and IDBs).

For each boundary type, $S_{V-\text{bin}}$ is determined from S_V^{GNB} (or S_V^{IDB}) multiplied by $n_{\text{bin}}^{\text{GNB}}/N_{\text{GNB}}$ (or $n_{\text{bin}}^{\text{IDB}}/N_{\text{IDB}}$), where $n_{\text{bin}}^{\text{GNB}}$ (or $n_{\text{bin}}^{\text{IDB}}$) is the number of boundaries in the bin and N_{GNB} (or N_{IDB}) is the total number of boundaries measured. The calculation is summarized in Eq. [7]:

$$E_{\text{TEM,dist}} = \left(\sum_{\text{bin}} \gamma_{\text{bin}}^{\text{GNB}}(\bar{\theta}_{\text{bin}}^{\text{GNB}}) \cdot n_{\text{bin}}^{\text{GNB}} \right) \frac{S_V^{\text{GNB}}}{N_{\text{GNB}}} + \left(\sum_{\text{bin}} \gamma_{\text{bin}}^{\text{IDB}}(\bar{\theta}_{\text{bin}}^{\text{IDB}}) \cdot n_{\text{bin}}^{\text{IDB}} \right) \frac{S_V^{\text{IDB}}}{N_{\text{IDB}}} \quad [7]$$

The values of S_V^{GNB} and S_V^{IDB} for each of the distributions are taken from separate TEM measurements (over a large area) of the average boundary spacings for the GNBs and IDBs. This method involves an implicit assumption that there is no correlation between each misorientation angle and the area per volume of boundaries with that misorientation angle. Both estimates are given in Table IV and are plotted as a function of strain in Figure 6, together with the weighted average of the DSC measurements.

Figure 6 shows a linear relationship between the stored energy based on the microstructure (E_{TEM}). A linear least squares fit to the data gives a proportionality constant between E_{TEM} and ε_{vM} of 1.6 or 1.7, where the lower value corresponds to the value obtained considering the complete misorientation angle distribution (method 2), rather than just the average values (method 1). In the following discussion, only data obtained using the distribution of misorientation angles are used. The DSC-measured stored energy (E_{DSC}) is also plotted in Figure 6, where it is seen to be consistently higher than the stored-energy estimate based on the microstructural data ($E_{\text{TEM,dist}}$). The ratio between the $E_{\text{TEM,dist}}$ and E_{DSC} at each strain level is given in Table V. From this, it is seen that the ratio $E_{\text{DSC}}/E_{\text{TEM,dist}}$ decreases with increasing strain.

C. Yield Stress

The measured yield stress is displayed as a function of strain in Figure 7. The stress-strain curve initially shows a parabolic increase up to a strain of $\varepsilon_{\text{vM}} \approx 1.0$, which is

Table V. Stored Energy Determined by DSC and TEM

	70 Pct	90 Pct	98 Pct
E_{DSC} (MJ/m ³)	8.9	12.1	15.8
$E_{\text{TEM,dist}}$ (MJ/m ³)	3.3	4.9	8.2
$E_{\text{DSC}}/E_{\text{TEM,dist}}$	2.7	2.5	1.9

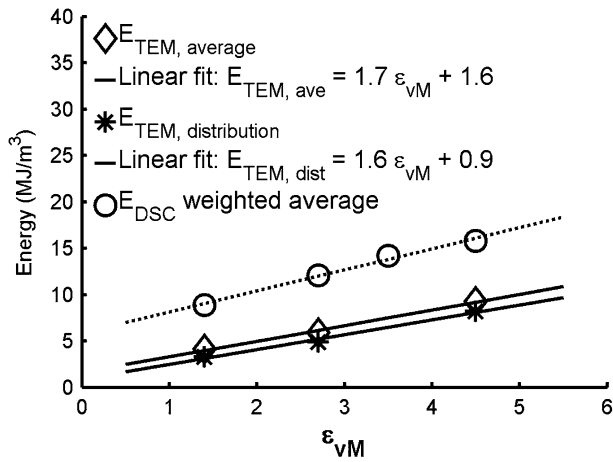


Fig. 6—Stored energy estimated from the microstructural TEM data. DSC data are also displayed.

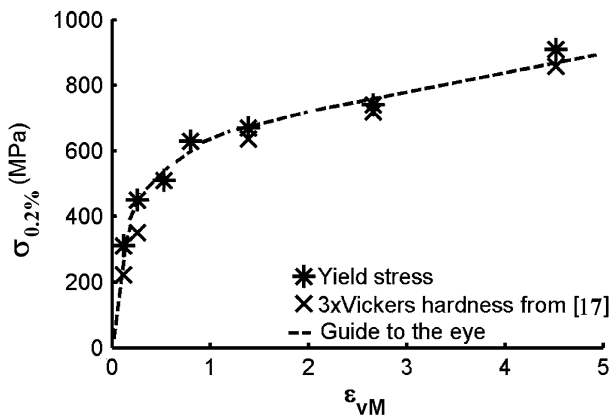


Fig. 7—Yield stress vs strain and 3 times Vickers hardness vs strain from Ref. 17.

characteristic of the stage III work-hardening regime. This is followed by a linear work hardening at larger strains, which is characteristic of the stage IV work-hardening regime. These observations are more clearly seen in Figure 8, where the work-hardening rate as a function of stress is displayed.

IV. DISCUSSION

A. Stored Energy—DSC

The energy stored in a deformed metal, in the most general case, can be thought of as arising from contributions from dislocations, high-angle boundaries, internal stresses, and point defects. The contribution to the stored energy of the point defects, if present, can be identified as a separate peak in a DSC measurement. In the present study, however, for both the Cu and Ni samples, the DSC measurements showed that the stored energy was released during heating in one stage (peak), which is related to the recrystallization of the samples (Figures 1 and 2). Thus, we can exclude point defects as a significant contribution to the stored energy. It is

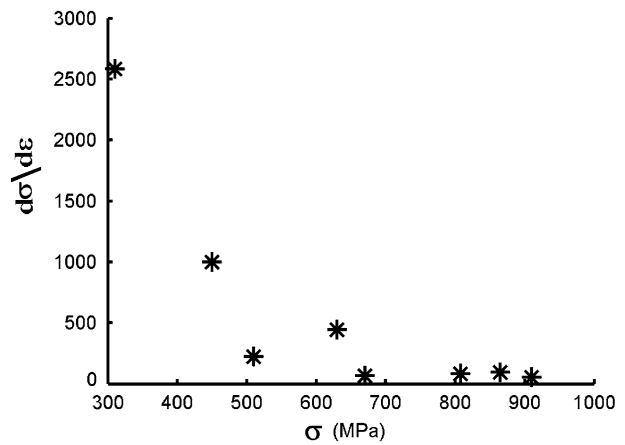


Fig. 8—Work-hardening rate as a function of stress.

suggested that the annihilation of such defects may have taken place already during deformation, due to the high purity of both copper and nickel.

The observation that, for Cu, the energy release takes place in one stage, due to recrystallization, is in agreement with findings reported elsewhere.^[1,4,5,24–26] Furthermore, the assumption that the energy release due to recovery is a minor effect is also supported by the findings of Reference 24, where the energy released during recovery of tensile-deformed (39.5 pct) high-purity copper (99.999 pct purity) was just 3 pct of the total stored energy. In the present study, the stored energy of copper cold rolled 90 pct was determined to be 6.9 MJ/m³. For commercial oxygen-free high conductivity (OFHC) copper (99.96 to 99.98 pct purity), deformed in compression at RT, the stored energy was found to be linearly related with the strain.^[4] From Figure 6 of Reference 4, the relationship between stored energy and strain can be expressed as $E(\text{cal/g}) = 0.0023 \varepsilon - 0.01$, where ε is the percent reduction. A 90 pct reduction corresponds, therefore, to a stored energy of 7.35 MJ/m³, which is just 4 pct higher than the value measured in the current study, *i.e.*, the two findings are very similar. Slightly lower values of 5.9 and 7.0 MJ/m³ were determined for 99.9996 pct pure copper with initial grain sizes of 15 and 50 μm cold rolled 93 pct in Reference 5, while in Reference 25, a somewhat lower stored energy for 90 pct cold rolled 99.99 pct pure copper of 4.22 MJ/m³ is reported.

The observation that, for deformed nickel, the energy release takes place by recrystallization in one stage has been reported in Reference 9. Other observations, however, carried out under different conditions, report up to three exothermic peaks during the heating of nickel.^[1,4,6,9,27] In these reports, the three peaks were related to the annihilation of vacancies, recovery, and recrystallization. Such an energy release was, for example, observed to take place in impure nickel (99.6 pct purity) deformed in torsion to $\varepsilon_{vM} = 2.56$ at RT.^[4] In that study, it was found that the energy release during the third stage, *i.e.*, recrystallization, was 6.7 MJ/m³, while the total energy release was 18.4 MJ/m³. In the current work, the total measured stored energy at

$\varepsilon_{vM} = 2.6$ is 11.9 MJ/m^3 , a value 35 pct lower. The difference between the values may be related to the difference in the purity of the metals, as it is known that the presence of impurities can increase the energy stored during plastic deformation.

In contrast, for 99.99 pct pure nickel cold rolled 90 pct,^[9] only one peak related to recrystallization was observed, with an energy release of 5.7 MJ/m^3 , lower than the value observed in the present work by a factor of 2, roughly. Because the purity of the nickel is similar to the one used in the current work, the rather large difference in stored energy cannot be attributed to a difference in purity. A possible explanation of the differences might, therefore, be different conditions during cold rolling.

The finding that stored energy increases linearly with strain in certain strain ranges has, furthermore, previously been observed in 99.99 pct copper,^[5,27] 99.99 pct pure nickel,^[9] and 99.999 pct pure silver.^[7]

Based on these data, therefore, the contributions to the stored energy are reduced to those from dislocations, high-angle boundaries, and internal stresses related to the microstructural features. Considering first the internal stresses, it has been suggested that these are minimized through a structural organization into LEDS.^[28] For such LEDS, it was furthermore suggested that internal stresses cannot exceed the flow stress, as stresses higher than this will be relaxed through yielding.^[28] Based on theoretical considerations, it has been shown that the energy stored due to internal stresses is significantly smaller than (approximately one-fifth of) the energy stored in the form of dislocations.^[29]

In the present study, the flow stress (0.2 pct offset) has been determined to be a function of strain (Figure 7). The stored energy caused by internal stresses can be calculated as the maximum elastic energy:

$$E_{\text{elastic}} = 0.5 \cdot \sigma \cdot \varepsilon_{vM} = 0.5 \cdot \frac{\sigma^2}{E_{\text{Young}}} \quad [8]$$

where σ is the flow stress, ε_{vM} the strain, and E_{Young} the elastic modulus of Ni (200 GPa ^[30]). In the strain range considered, the flow stress increases from 670 (70 pct) to 910 MPa (98 pct); hence, the contribution from the internal stresses is about 25 to 35 pct of E_{TEM} and is roughly in agreement with the theoretical prediction.^[29]

B. Stored Energy—TEM

The parameters characterizing the deformation structures in Ni have been determined from Kikuchi line measurements in a TEM. An alternative method would be to use the electron backscattering diffraction (EBSD) technique.^[12,14] The limited angular resolution of this method (up to 2 deg for heavily deformed samples) results, however, in a number of low-angle boundaries being undetected in an investigation of a deformed sample. As a result, a stored-energy analysis based on EBSD data will lead to an underprediction, with the error being larger at smaller applied strains. For large strains, the two methods may give comparable results.^[12] In the present study, the TEM method was

chosen for all samples, in order to facilitate the comparison of data over the entire strain range.

The stored energy has been calculated using the Read–Shockley formalism, as expressed in Eq. [2]. This equation includes the energy stored in the dislocations and the dislocation core, but excludes the contribution of internal stresses caused by the presence of the dislocations.^[20] The structure of the deformed Ni, as previously described, contains dislocation boundaries and high-angle boundaries ($> 15 \text{ deg}$), where the latter includes both those present in the starting material and those introduced during cold rolling. The contribution from the high-angle boundaries is taken into account through the grain-boundary energy (Eq. [2]). For samples deformed to large strains, this contribution may account for a large fraction of the stored energy, as the fraction of high-angle boundaries may be as high as 60 to 80 pct.^[31] In the present experiment, the fraction of high-angle boundaries increases from 7 to 28 pct as the rolling reductions is increased from 70 to 98 pct.

In the calculation of E_{TEM} based on the Read–Shockley equation, the contribution from dislocations stored between boundaries has not been included. The density of such dislocations has been estimated in Reference 19 to be about 10^{14} m^{-2} , or one dislocation per cell at a reduction strain of 98 pct. The energy associated with these loose dislocations (E_{Loose}) can be calculated from the relationship

$$E_{\text{Loose}} = 1/2 \cdot \rho \cdot G \cdot \mathbf{b}^2 \quad [9]$$

where G is the shear modulus, \mathbf{b} is the length of the Burgers vector, and ρ is the dislocation density. Taking values for nickel of $G = 79 \text{ GPa}$ ^[32] and $b = 0.249 \text{ nm}$ ^[33] gives the stored energy of loose dislocations as 0.24 MJ/m^3 . This value corresponds to a mere 3 pct increase in strain, an insignificant contribution in the present sample.

C. Comparison of E_{DSC} and E_{TEM}

A comparison of E_{DSC} and E_{TEM} shows that the ratio $E_{\text{DSC}}/E_{\text{TEM,dist}}$ is 1.9 to 2.7 and decreases with increasing strain (Table V). If, however, stored-energy values calculated based on average misorientations angles are used, the ratio $E_{\text{DSC}}/E_{\text{TEM,av}}$ decreases to 1.7 to 2.1. Additionally, if the contribution of internal stresses is included to $E_{\text{TEM,dist}}$, the fraction $E_{\text{DSC}}/E_{\text{TEM,dist}}$ is reduced to 1.5 to 2. A comparable discrepancy between E_{DSC} and E_{TEM} has been observed in previous studies.^[1,2,15] For example, in a recent study of polycrystalline copper deformed by cold rolling in the strain range 1 to 3,^[16] the dislocation density derived on the basis of calorimetry data was higher by a factor of 1.5 to 2 than the dislocation density determined from the X-ray line profile analysis.

For this discussion, we assume that E_{DSC} is taken as the most correct estimate of the stored energy and discuss why the E_{TEM} value is lower. Consider first that the dislocation density is not determined directly in the TEM characterization; instead, the dislocation density is estimated based on the assumption that the dislocations

are organized in rotation boundaries with a misorientation angle θ . For such boundaries, the area density of dislocations stored in the boundary is of the order of θ/b . In most cases, θ/b gives a minimum number for the dislocation density, because some dislocations may screen each other (*i.e.*, $+b$ and $-b$) and thus not contribute to θ .^[28] These redundant dislocations have an average density of $1/h - \theta/b$, where h is the average distance between all the dislocations in a boundary. Such redundant dislocations may be present in significant numbers at low strain, whereas with the increasing perfection of boundaries at larger strain, their contribution will decrease. Such a reduction will be reflected in a decrease in the ratio E_{DSC}/E_{TEM} with increasing strain, as observed (Table V). An example of a boundary with no redundant dislocations is illustrated in a high-resolution electron microscope (HREM) micrograph^[34] of copper deformed to large strain (Figure 9(a)). For such boundaries, the individual dislocations can be identified and the distance between the dislocations, h , can be determined, allowing the area density of dislocations to be calculated as $1/h$. For the boundary in Figure 9(a), there is good agreement between the two area densities $1/h$ and θ/b , showing that the dislocation density in the boundary can be accounted for solely on the basis of the misorientation angle. Extra dislocations may, however, also be present in some boundaries, as illustrated in Figure 9(b) (also from Reference 34). The presence of such dislocations near or at boundaries has also been observed in conventional TEM studies,^[17] and will contribute to the stored energy measured by DSC, but not to that calculated from the microstructure.

Extra dislocations may also be present in the regions near the high-angle boundaries. However, HREM observations of high-angle boundaries in the deformed metal show that such boundaries have the same characteristics as grain boundaries in undeformed metals. As a consequence, the energy of all high-angle boundaries in Eq. [2] can be taken as γ_m , and the contribution of these boundaries added to the contribution from the dislocation (< 15 deg misorientation) boundaries. It is,

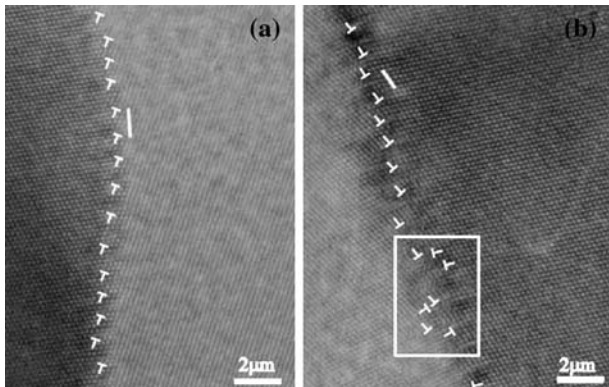


Fig. 9—High-resolution transmission electron microscopy of low-angle boundaries in Cu (99.99 pct) from Ref. 34. (a) 11-deg low-angle boundary, well described by edge dislocations and (b) 14-deg low-angle boundary described partly by edges dislocations and partly by random edges dislocations, emphasized in the white box.

however, a characteristic of deformed microstructures that the dislocation boundaries and high-angle boundaries are interconnected at triple lines. Such an interconnection is illustrated in Figure 2 in Reference 35. It may, therefore, be hypothesized that these interconnections are associated with an additional amount of stored energy in the microstructure. The magnitude of such junction energies is, however, a subject for further work.

To summarize the discussion of the TEM and DSC stored energy, the measured stored energy is higher initially by a factor of 2.7, compared to the stored energy calculated from the microstructure. This difference decreases to a factor of 1.9 in the stage IV work-hardening regime. If internal stresses are considered, and if a general uncertainty of 20 pct in the experimental data is assumed, the stored-energy values measured with the two methods approach each other with increasing strain, as illustrated in Figure 10.

D. Stored Energy and Flow Stress

In the present study, the flow stress has been determined for samples deformed over a large strain range, from 0.12 to 4.5 (Figure 7). Hardness measurements for the nickel material characterized by TEM are also given.^[17] A fairly good agreement is seen between the two sets of data. Initially, the stress-strain curve displays a predominant stage III work-hardening regime, which is followed at a strain of ≈ 1 by a stage IV work-hardening regime. The stored energy has only been measured at large strains for which a linear relationship with strain was obtained (Figure 4).

The linear relationship at large strains is used to calculate the ratio between the stored energy and the expended energy. This ratio can be calculated in different ways. In the following, it is estimated as the instantaneous increase in stored energy, from the plastic work, expressed by the equation

$$W = \int \sigma d\varepsilon \quad [10]$$

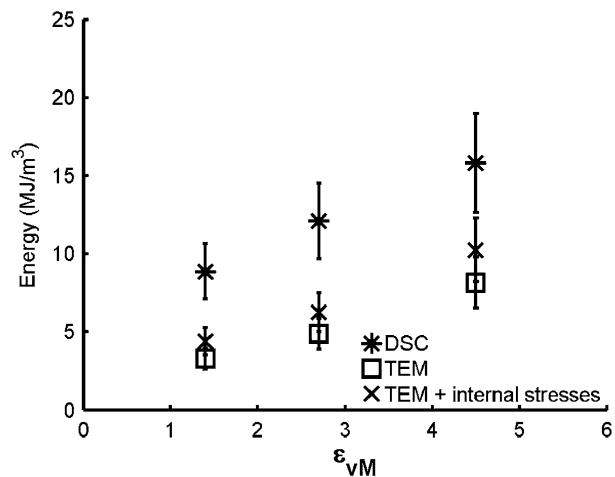


Fig. 10—Stored energy as a function of strain. Measured by DSC and evaluated by TEM.

where W is the plastic work, σ is the flow stress, and ε the strain. The stress in stage IV can be expressed by the equation

$$\sigma = \sigma_0 + \Theta\varepsilon \quad [11]$$

where Θ is the work-hardening rate and σ_0 the extrapolated flow stress at $\varepsilon = 0$. From Eqs. [10] and [11], we can write

$$W = \sigma_0\varepsilon + 1/2\Theta\varepsilon^2 \quad [12]$$

The experiments show that a linear relationship exist between the stored energy and the strain:

$$E = E_0 + m\varepsilon \quad [13]$$

where E_0 is the extrapolated stored energy at $\varepsilon = 0$ and m is the proportionality constant between E and ε . If the instantaneous energy storage ratio is defined as

$$\beta = \frac{dE}{dW} \quad [14]$$

the value of β can be found from Eqs. [12] and [13]:

$$\beta = \frac{dE}{d\varepsilon} / \frac{dW}{d\varepsilon} = \frac{m}{\sigma} \quad [15]$$

In the current work, $m = 2.3$ and $\sigma \in [670 \text{ to } 910]$; therefore, $\beta \in [0.002 \text{ to } 0.003]$. This means that, initially, between stage III and stage IV, 0.3 pct of the expended energy is stored in the metal and, later, in stage IV, this drops to 0.2 pct.

Alternatively, the instantaneous ratio of the total stored energy to the total expended work can be calculated. By doing so, it is found that, at a reduction of 70 pct, just 1.2 pct of the plastic work is stored in the metal, whereas at 98 pct, only 0.5 pct is stored, *i.e.*, the energy stored decreases in the stage IV work-hardening regime. This decrease may be directly related to the way dislocations are stored in the two stages. In stage III, the dislocations are primarily stored in dislocations boundaries, while in stage IV, the structures contain an increasing density of deformation-induced high-angle boundaries, which may be better able to absorb and annihilate dislocations during deformation. As a result, the rate of increase in the dislocation density and in the stored energy will be smaller in stage IV than in stage III.

V. CONCLUSIONS

The stored energy in high-purity (99.99 pct) Ni, cold rolled to equivalent von Mises strains of 1.4 to 4.5 (70 to 98 pct thickness reduction), has been determined by DSC and also estimated based on a quantitative microstructural characterization from TEM data by applying the Read-Shockley equation. The conclusions are the following.

1. The stored energy measured by calorimetry is higher by a factor of 1.9 to 2.7 than the value based on an estimate of the energy stored in dislocation

boundaries and high-angle boundaries. This discrepancy can be reduced by introducing contributions both from dislocations stored between the boundaries and from internal stresses.

2. The stored energy determined both by calorimetry and microscopy increases linearly with strain in the strain range examined. In this interval, the flow stress also increases linearly with strain (stage IV work hardening).
3. The ratio between the stored energy and the expended energy is small in stage IV and decreases with increasing strain.
4. The consistency between values obtained in this comparative study validates both the calorimetric and the microstructure-based techniques. The former may be preferred for bulk analysis, whereas the latter is preferable for an analysis of local variations in the stored energy, due to heterogeneities in the deformed microstructure, which are important for the recovery and recrystallization behavior during subsequent annealing.

ACKNOWLEDGMENTS

Two of the authors (TK and NH) gratefully acknowledge the Danish National Research Foundation for supporting the Center for Fundamental Research: Metal Structures in Four Dimensions, within which this work was performed. Two other authors (AG and QL) acknowledge the National Natural Science Foundation of China for financial support under Contract Nos. 50571049 and 50571051. The authors are also grateful to Dr Wolfgang Pantleon for his help in full discussions and for proposing the use of Eq. [11].

REFERENCES

1. M.B. Bever, D.L. Holt, and A.L. Titchener: *Prog. Mater. Sci.*, 1973, vol. 17, pp. 1–177.
2. D. Rönnpagel and C. Schwink: *Acta Metall.*, 1978, vol. 26, pp. 319–31.
3. E. Woldt and D. Juul Jensen: *Metall. Trans. A*, 1995, vol. 26A, pp. 1717–24.
4. L.M. Clarebrough, M.E. Hargreaves, and G.W. West: *Proc. R. Soc. London, Ser. A*, 1955, vol. 232, pp. 262–70.
5. B. Hutchinson, S. Jonsson, and L. Ryde: *Scripta Metall.*, 1989, vol. 23, pp. 671–76.
6. F. Bell: *Arch. Eisenhüttenwesen*, 1965, vol. 36, pp. 745–49.
7. A. Zahia, F. Salhi, J. Aride, D. Monya-Siesse, and G. Moya: *J. Alloys Compd.*, 1992, vol. 188, pp. 264–67.
8. R.O. Williams: *Trans. TMS-AIME*, 1962, vol. 224, pp. 719–26.
9. I. Baker, L. Liu, and D. Mandal: *Scripta Metall.*, 1995, vol. 32 (2), pp. 167–71.
10. F. Bell and O. Krisement: *Acta Metall.*, 1962, vol. 10, pp. 80–83.
11. L.M. Clarebrough, M.E. Hargreaves, and G.W. West: *Philos. Mag.*, 1953, vol. 44, pp. 913–15.
12. A. Godfrey, W.Q. Cao, N. Hansen, and Q. Liu: *Metall. Mater. Trans. A*, 2005, vol. 36A, pp. 2371–78.
13. A. Godfrey, N. Hansen, and D. Juul Jensen: *Metall. Mater. Trans. A*, 2007, vol. 38A, pp. 2329–39.
14. A. Godfrey, Q. Liu, D. Juul Jensen, and N. Hansen: *Proc. 25th Riso Int. Symp.*, C. Gundlach, K. Haldrup, N. Hansen, X. Huang, D. Juul Jensen, T. Leffers, Z.J. Li, S.F. Nielsen, W. Pantleon, J.A. Wert, and G. Winther: 2004, pp. 317–22.

15. T. Ungar, H. Mughrabi, D. Rönnpagel, and M. Wilkens: *Acta Metall.*, 1984, vol. 36, pp. 333–42.
16. T. Ungar, E. Schafler, P. Hanák, S. Bernstorff, and M. Zehetbauer: *Mater. Sci. Eng., A*, doi:[10.1016/j.msea.2006.03.156](https://doi.org/10.1016/j.msea.2006.03.156).
17. D.A. Hughes and N. Hansen: *Metall. Trans. A*, 1993, vol. 24A, pp. 2021–37.
18. *The Periodic System of the Elements*, Linde Press, Aarhus, Denmark, 1993.
19. D.A. Hughes and N. Hansen: *Acta Mater.*, 2000, vol. 48, pp. 2985–3004.
20. W.T. Read and W. Shockley: *Phys. Rev.*, 1950, vol. 78, pp. 275–89.
21. L.E. Murr: *Interfacial Phenomena in Metals and Alloys*, Addison-Wesley, London, 1975, Chap. 3.
22. A. Godfrey and D.A. Hughes: *Mater. Charact.*, 2002, vol. 48, pp. 89–99.
23. A. Godfrey and D.A. Hughes: *Acta Mater.*, 2000, vol. 48, pp. 1897–1905.
24. P. Gordon: *Trans. AIME*, 1955, vol. 203, pp. 1043–52.
25. D. Mandal and I. Baker: *Scripta Metall.*, 1995, vol. 33 (5), pp. 831–36.
26. G. Gottstein, H. Steffen, and H. Wollenberger: *Scripta Metall.*, 1973, vol. 7, pp. 451–56.
27. D. Michell and E. Lovegrove: *Philos. Mag.*, 1960, vol. 5, pp. 499–518.
28. D. Kuhlmann-Wilsdorf: *Mater. Sci. Eng., A*, 1989, vol. 113, pp. 1–41.
29. N. Hansen and D. Kuhlmann-Wilsdorf: *Mater. Sci. Eng.*, 1986, vol. 81, pp. 141–61.
30. *Hütte, Des Ingenieurs Taschenbuch Theoretische Grundlagen*, 28th edition, Verlag von Wilhelm Ernst & Sohn, Berlin, 1955, p. 1048.
31. O.V. Mishin, D. Juul Jensen, and N. Hansen: *Mater. Sci. Eng., A*, 2003, vol. A342, pp. 320–28.
32. N. Hansen: *Scripta Mater.*, 2004, vol. 51, pp. 801–06.
33. J.S. Koehler: *Phys. Rev. B*, 1970, vol. 2 (2), pp. 547–51.
34. K. Ikeda, K. Yamada, N. Takata, F. Yoshida, H. Nakashima, and N. Tsuji: *Proc. 25th Riso Int. Symp.*, C. Gundlach, K. Haldrup, N. Hansen, X. Huang, D. Juul Jensen, T. Leffers, Z.J. Li, S.F. Nielsen, W. Pantleon, J.A. Wert, and G. Winther, eds., Risoe National Laboratory, Roskilde, Denmark, 2004, pp. 357–62.
35. A.R. Jones, B. Ralph, and N. Hansen: *Proc. R. Soc. London, Ser. A*, 1979, vol. 368, pp. 345–57.